DOI: 10.1002/ ((please add manuscript number))
Article type: Full Paper

Roles of Interfacial Tension in Regulating Internal Organization of Low Bandgap Polymer Bulk Heterojunction Solar Cells by Polymer Additives

Zhenhua Yang, Yichen Guo, Hongfei Li, Yuchen Zhou, Xianghao Zuo, Yingjie Yu, Cheng Pan, Joseph Strzalka, Chang-Yong Nam, and Miriam H. Rafailovich**

Dr. Z. Yang, Y. Guo, Dr. H. Li, Y. Zhou, X. Zuo, Y. Yu, Dr. C. Pan, Prof. M. H. Rafailovich
Department of Materials Science and Chemical Engineering, Stony Brook University, Stony Brook, NY 11794, USA
E-mail: miriam.rafailovich@stonybrook.edu
Dr. C.-Y. Nam
Center for Functional Nanomaterials, Brookhaven National Laboratory, Upton, NY 11973, USA
E-mail: cynam@bnl.gov
Dr. J. Strzalka
X-ray Science Division, Argonne National Laboratory, Argonne, IL 60439, USA

Keywords: low bandgap polymer solar cells, ternary blends, polymer additives, interfacial tension, crystallinity

The role of a tertiary polymer-based additive was investigated in increasing the efficiency of inverted low bandgap polymer:fullerene bulk heterojunction (BHJ) solar cells. Charge separation in polymer BHJ solar cells relies on the phase separation between electron accepting fullerene derivatives and photoactive polymers. Proper distribution of individual phases of suitable crystallinities within the active layer is a key factor for efficient charge transport/extraction and high photovoltaic performance. Here, it is demonstrated that the minor addition of a tertiary amorphous polymer, polystyrene (PS), with optimized molecular weights can increase the overall photovoltaic efficiency of poly[N-9′-heptadecanyl-2,7-carbazole-alt-5,5-(4′,7′-di-2-thienyl-2′,1′,3′-benzothiadiazole)]:phenyl-C_{61}butyric acid methyl ester (PCDTBT:PCBM) inverted BHJ solar cells, through the interfacial-tension-driven increase in crystallinities of photoactive phases and redistribution of PCBM molecules away from the top hole-collecting anode interface. Complementary studies correlating polymer

interfacial tension, blend internal structure, charge transport, and photovoltaic characteristics show that tertiary, high molecular-weight polymers can serve as effective additives for improving the performance of low bandgap polymer solar cells.

1. Introduction

Bulk heterojunction (BHJ) solar cells have been extensively studied due to their flexibility and potential toward high-throughput roll-to-roll fabrication.[1] Recently, most of the high-efficiency polymer:fullerene BHJ solar cells have adopted an inverted device structure, where metal oxides, such as TiO_2 or ZnO, are used as the electron-selective buffer layer on a transparent conducting oxide (e.g., indium tin oxide (ITO)) substrate, instead of the normal structure that uses the corrosive and hygroscopic hole-selective poly(3,4-ethylenedioxylenethiophene):poly(styrenesulphonic acid) (PEDOT:PSS).[2] By avoiding the usage of PEDOT:PSS and low-work-function top metal cathode, inverted devices achieve better long-term ambient stability than normal type devices.[3]

Morphology control of the active layer in BHJ solar cells has been shown to be an essential consideration which could improve the power conversion efficiency (PCE).[4] The active BHJ layer usually consists of an interpenetrating network of electron-donating conjugated polymers and electron-accepting fullerenes.[5] Important factors that must be considered when optimizing the morphology of BHJ active layer include: a) Miscibility between donor and acceptor materials; b) Size, composition, and crystalline characteristics of phase-separated domains; c) Presence of percolating charge transport networks; and d) Vertical concentration gradient.[6] In particular, the use of BHJ with favorable compositional gradient in the vertical direction to establish the charge selectivity at electrodes have been proposed as an effective approach to enhance the efficiency of polymer solar cells, regardless of the types of donor and acceptor materials.[7] Specifically, the preferential segregation of the polymer donor to the anode-active layer interface can block electrons and enhance hole

collection, leading to the enhanced short circuit current density and improved device performance. In contrast, the segregation of fullerenes to the interface between anode and active BHJ layer can dramatically increase the device series resistance and block the hole transport and extraction, resulting in decreased device performances.[8] The segregation of the electron acceptor phase can be controlled within the blend by the addition of a tertiary component. Our previous work has shown that the addition of a tertiary polymer component could lead to the spontaneous formation of vertical columns within BHJ films and template the PCBM segregation at the column surface, thereby creating a direct pathway to the electrode and improving device photovoltaic performance.[4a],[9] This method however introduced a large volume fraction of non-photoactive component (~33 %), which decreased the volume of photoactive phases in the BHJ film.

Sun et al.[10] have shown that the addition of small amounts (5 wt.%) of block copolymers as a tertiary phase in the poly(3-hexylthiophene-2,5-diyl) (P3HT):PCBM blend could decrease the interfacial tension between P3HT and PCBM, preventing the layering (i.e., excessive segregation) of the PCBM at the film surface. This method was shown to significantly increase the solar cell PCE since it minimized the volume of inert phase while facilitating the improvement of BHJ morphology favorable for the efficient collection of photogenerated charge carriers. However, the large bandgap of P3HT (~1.9 eV) restricts its absorbance to wavelengths below 650 nm, thereby fundamentally limiting a further enhanced PCE.[11] An extensive research effort has been focused on extending the absorption spectrum of organic solar cells via, such as, the ternary BHJ systems, with the recent reports by Xiao et al.[12] and Li et al.[13] demonstrating impressive over 12% PCE with a near infrared spectral coverage (over 1000 nm) by introducing new organic, non-fullerene electron acceptors. More major approach has been centered on developing various low-bandgap polymer electron donors, such as poly[N-9′-heptadecanyl-2,7-carbazole-alt-5,5-(4′,7′-di-2-thienyl-2′,1′,3′-benzothiadiazole)] (PCDTBT), to replace P3HT.[14] However, since the interfacial energies

between the low-bandgap polymer, such as PCDTBT, and PCBM are very different from those in the P3HT:PCBM blends, the internal morphology of BHJ film is also very different, and new approaches must be developed in order to find the structure that optimize the efficiency. In contrast to P3HT, PCDTBT is far more miscible with fullerenes and other polymers, making it more difficult to achieve a phase-separated morphology and, thus, requiring a much larger volume fraction of PCBM (e.g., polymer:fullerene blend ratio of 1:4).[14] In this blend, the challenge is therefore to *increase immiscibility* and sharpen interfacial contrast, while preventing the excessive segregation of domains. Hence, the tertiary additive approaches that increased the efficiency of P3HT:PCBM blends would not work in this case since they target the reduction of the interfacial tension, rather than its increase.

It is well established that the immiscibility between polymers can be enhanced with increasing molecular weight.[15] Huang et al.[16] demonstrated that the addition of small amounts of high-molecular-weight polystyrene (PS) acted as surfactants, which stabilized the blend of 7,7′-(4,4-bis(2-ethylhexyl)-4H-silolo[3,2-b:4,5-b′]dithiophene-2,6-diyl)bis(6-fluoro-4-(5′-hexyl-[2,2′-bithiophene]-5-yl)benzo[c][1,2,5]thiadiazole) (p-DTS(FBTTh$_2$)$_2$) *small molecules* and PCBM against dewetting, enabling the spin-casting of thicker films with larger crystalline domains. In contrast, in the BHJ consisting of *low-bandgap polymer*, such as PCDTBT, and PCBM, the internal structure is more complicated since the crystallinity of polymer phase is determined by both chain folding and nucleation, which in turn also control its interfacial properties with PCBM. For example, as the polymer crystallizes, the PCBM phase is typically expelled and segregates to the free film surface. This can enhance the electron charge transfer to the cathode in normal-type devices but interferes with hole transfer at the anode in inverted devices, causing the charge recombination and subsequent decrease in PCE. We postulate that, driven by high interfacial tension, a small fraction of *high molecular weight PS* added to the PCDTBT:PCBM BHJ blend may generate a BHJ internal morphology favorable for enhancing the device photovoltaic performance: In this case, the PS phase, due

to its high immiscibility with PCDTBT and PCBM, would segregate into small dispersed domains within the BHJ active layer, analogous to a well-dispersed particle mixture, forming multiple nucleation sites for crystalline PCDTBT polymer domains, increasing the polymer crystallinity. At the same time, the tertiary PS with high surface tension can also naturally segregate toward the free surface to potentially alleviate the top-surface segregation of PCBM in the BHJ film and render the local BHJ composition near the top electrode more balanced, enabling the more efficient hole collection and, subsequently, enhanced PCE in the inverted solar cell. Despite these potential prospects, the impact of high molecular weight, tertiary polymers as an additive to the structural, charge transport, and photovoltaic characteristics in low-bandgap polymer:fullerene BHJ solar cells has not been adequately studied.

In this study, we investigate the effects of adding small amounts of PS with various molecular weights on the internal structure, charge transport, and photovoltaic performance of BHJ blend consisting of low-bandgap PCDTBT polymer and PCBM. Specifically, we experimentally determine the PS-molecular-weight-dependent interfacial tension among the BHJ components and establish its correlation with the vertical compositional gradient, polymer crystalline structure, charge carrier mobility, and ultimate device photovoltaic characteristics of PCDTBT:PCBM inverted BHJ solar cells. The results confirm the enhancement of PCE by up to 21 % in the PCDTBT:PCBM BHJ solar cell via the addition of a small amount (2.5 wt.%) of high molecular weight PS (>2M Da), primarily due to the interfacial tension that induces the nucleation of PCDTBT crystalline domains, enhancing the hole conduction through the active blend layer. The vertical compositional profile further reveals that the addition of minor PS also prevents the aggregation of electron acceptor PCBM at the interface between active BHJ blend layer and top anode, contributing to the improvement of overall device PCE. The elucidated influences of high-molecular-weight polymer additives on the performance of low-bandgap polymer:fullerene BHJ solar cells advance the fundamental understanding on the correlation between the polymer interfacial

tension, and structural and charge transport characteristics of the active BHJ layer, providing a useful guideline for using polymer additives toward developing high-performance organic polymer solar cells.

2. Results and Discussion

2.1. Photovoltaic Performance on PCDTBT:PCBM BHJ Solar Cells with PS Additives

2.1.1. PS Concentration Dependence

We first measured the photovoltaic performance of PCDTBT:PCBM inverted BHJ solar cells as a function of concentration of PS (molecular weight (MW) = 2M Da) added in the active blend. The high MW of PS was chosen to ensure the phase separation between the two polymer phases in the BHJ layer as we discuss in detail later. The results are shown in **Figure 1**a, where the photovoltaic current density–voltage (J–V) response of PCDTBT:PCBM BHJ solar cells (1:4 blend ratio with ~90 nm film thickness) is plotted as a function of the added PS concentration ranging from 0 to 5 wt.%. The summary of measured average photovoltaic performance parameters for the various concentrations of PS is given in Table 1. When PCE is plotted as a function of PS concentration (Figure 1b), we find that there exists an optimal PS concentration for the maximized PCE, of around 2.5 wt.%: The average PCE increased by ~21 %, to 5.74 % from 4.75 % of control device without added PS, primarily driven by the simultaneous enhancements in short circuit current density (J_{sc}) and fill factor (FF) by 11 % and 5 %, respectively (Table 1). The open circuit voltage (V_{oc}) remained largely constant with varying PS concentration (only by ~10 mV increase at 2.5 wt.% PS concentration). The observed optimal PS concentration of 2.5 wt.% is roughly the same value reported by Huang,[16] which led to the formation of dispersed small spherical PS phase in the blend of p-DTS(FBTTh$_2$)$_2$) small molecules and PCBM. Meanwhile, increasing the PS concentration beyond 2.5 wt.% decreases the PCE (Figure 1b).

The optimal PS concentration we observed here is much smaller than that in P3HT:PCBM BHJ solar cells. Previously Pan et al. [4a] as well as Vohra et al. [17] have shown that the

efficiency of P3HT:PCBM BHJ solar cells could be increased by adding ~33 wt.% of tertiary photo-inert PS phase (i.e., with a blend ratio of 1:1 with P3HT by wt.). In their cases, the high volume fraction of PS induced the formation of a segregated PS columnar structure, which templated the PCBM phase, creating a direct pathway toward the electron-collecting cathode and, subsequently, reducing the internal ohmic resistance and recombination rate.[4a] The columns were also shown to enhance the nucleation of the face-on-oriented P3HT lamellar structure, thereby increasing the hole mobility.[17] In the case of PCDTBT:PCBM blend, the side chains of PCDTBT are much longer, making the polymer more miscible with PCBM, necessitating a four-fold increase in the amount of PCBM to be blended with PCDTBT (i.e., PCDTBT:PCBM blend ratio of 1:4) to generate a suitable phase-separated morphology for high photovoltaic performance.[14] These differences indicate that the internal structure of PCDTBT:PCBM blend is very different from that of P3HT:PCBM. In fact, if the PS concentration was increased to 20 wt.%, a large enough amount likely to induce the formation of PS columnar structure, the photovoltaic performance of PCDTBT:PCBM solar cells rather decreased significantly (Figure S1 and Table S1), again suggesting a dissimilar internal structure in the PCDTBT:PCBM blend compared with that of P3HT:PCBM blend. Considering the relatively smaller volume fraction of photoactive polymer in the PCDTBT:PCBM blend, the addition of large amount of photo-inert additives in the blend is not favorable, and the observed enhancement in photovoltaic performance by adding a small amount of PS is therefore a desirable advantage.

2.1.2. PS MW Dependence

MW of the polymer additive is another important factor that determines the final, phase-separated internal morphology and associated photovoltaic performance of a polymer:fullerene BHJ blend because of its known influence on the interfacial tension between polymers. To examine the effects of MW, the photovoltaic performance of PCDTBT:PCBM BHJ blend solar cells with PS additive has been measured as a function of

PS MW (from 50k Da to 7M Da) under the fixed PS concentration at 2.5 wt.%. The representative J–V characteristics for this set of experiments are shown in **Figure 2**a, and the average photovoltaic performance parameters are summarized in Table 2. Upon the addition of PS with the lowest MW (50k Da), the solar cell shows a PCE lower than that of the control device without PS by ~29 % (3.36 % versus 4.75 % on average, Table 2). However, with increasing PS MW, the PCE increases, eventually surpassing that of control device and becoming largely plateaued at ~5.7 % once the MW is larger than 2M Da (Figure 2b upper panel). This asymptotic increase of PCE with increasing PS MW is driven by the similar variations in J_{sc} and FF, which increase for a larger PS MW and saturate at ~11 mA/cm^2 and ~0.60, respectively for MW ≥ 2M Da (Table 2). In contrast, V_{oc} stays relatively insensitive to the PS MW in the blend.

We find that there is an PS-MW-dependent increase in hole mobility through the PCDTBT network in PCDTBT:PCBM BHJ blend, commensurate to the observed enhancement of device photovoltaic performance with increasing PS MW. The hole mobility was measured as a function of the MW of added PS using hole-only devices consisting of a PCDTBT:PCBM blend layer sandwiched between PEDOT:PSS and MoO_3 bottom and top hole-selective contacts, whose measured J–V characteristics were fitted with the Mott–Gurney equation.[18] The results clearly show that the hole mobility initially increases with increasing PS MW and saturates at the maximum value of ~1.75×10^{-4} cm^{-2}v^{-1}s^{-1} for MW ≥ 2M Da (Figure 2b lower panel), which is a five-fold increased value compared with that of the control BHJ blend without PS (Table 2). In addition, the MW-dependent increase of hole mobility is asymptotic, identical to the trend observed for PCE (Figure 2a); the rapid increases of both hole mobility and PCE for low PS MW (< 2M Da) are followed by plateaus for MW ≥ 2M Da. Meanwhile, the electron mobility through the PCBM network in PCDTBT:PCBM BHJ blend increases to a relatively modest degree with increasing PS MW (Figure 2b lower

panel), hinting that the hole transport through the polymer phase in PCDTBT:PCBM BHJ blend is more prominently affected by the structural change induced by PS additive.

2.2. Effects of PS Additives on the Internal Structure of PCDTBT:PCBM BHJ Blend

Considering that the variation in charge mobility in a polymer:fullerene BHJ blend is generally correlated with the internal structure (e.g., phase domain distribution, crystallinity etc.), the structural characteristics of PCDTBT:PCBM BHJ blend film was investigated by glancing incidence wide angle X-ray scattering (GIWAXS) as a function of the MW of PS additive. **Figure 3** shows the two-dimensional (2D) GIWAXS spectra and **Figure 4** associated one-dimensional (1D) GIWAXS profiles obtained by either surface or film mode (i.e., the incident angle (α) is larger than the critical angle (α_c) or vice versa with α_c = 0.13° for PCDTBT; see Experimental Section) from the PCDTBT:PCBM BHJ blend films containing 2.5 wt.% PS of different MWs. The GIWAXS spectra obtained by surface mode are sensitive to the structure near the PCDTBT:PCBM BHJ blend film surface, while the spectra by film mode to the structure in the interior of blend film. It is found that regardless of the added PS MW (50k, 1M, and 2M Da) or GIWAXS mode, the 2D GIWAXS spectra feature broad and isotropic (along the azimuth angle, ω), diffuse scattering rings at q = ~0.7 $Å^{-1}$, ~1.38 $Å^{-1}$, and ~2.0 $Å^{-1}$ (Figure 3), which typically correspond to the crystalline PCBM domains.[19] There is a significant increase in the intensities of the first and second-order scattering rings after adding high MW PS (>1 M Da) in the blend film as shown in the 1D line cuts of 2D GIWAXS intensity profiles (Figure 4), particularly to a greater extent near the surface (Figure 4a and 4b upper panels) compared with the interior bulk of film (Figure 4a and 4b lower panels). Considering that the scattering peak area above its background is generally influenced by the crystalline fraction of scattering domain, this suggests that the crystallinity of PCBM domains has increased by the added high MW PS, especially near the BHJ blend film surface.

Meanwhile, the scattering feature originating from the edge-on lamellar stacking of PCDTBT appears at q = ~0.4 $Å^{-1}$ [20] and shows a similar intensity increase, again more so near the surface, after adding high MW PS (>1 M Da) in the blend film (Figure 4b), indicating the increased crystallinty in the PCDTBT domains near surface as well. Consistently, the integrated scattering peak areas obtained by Gaussian fitting at q = ~0.4 $Å^{-1}$ (deconvoluted; see Figure S2 in Supporting Information) and ~1.38 $Å^{-1}$, which qualitatively represent the crystallinities of PCDTBT and PCBM respectively, increased simultaneously by over 600 % near the surface once the MW of added PS is over 1M Da (**Figure 5**a; also see Table S2 and S3). This large increase in phase crystallinities near the surface is in contrast to their relatively modest increases within the film under the increasing PS MW (less than ~60 % and ~80 % for PCDTBT and PCBM, respectively; Figure 5a). The increased areas of PCBM and PCDTBT scattering peaks were accompanied by the increase in their full width at half maximum (FWHM) as the MW of added PS increases, both near the surface and within the film (Figure S3; also see Table S2 and S3). Based on the Scherrer equation,[21] this corresponds to the slight decrease of coherence length (i.e., crystalline domain size) for both PCBM (from ~4.4 nm to ~4 nm) and PCDTBT (from ~3.6 nm to 3 nm) throughout the BHJ film as the MW of added PS increases (Figure 5b), expect for the PCBM domain near the surface that show a somewhat recovering coherence length for PS MW = 2M Da. The overall decreased crystallite sizes of both PCDTBT and PCBM phases by the addition of PS, combined with their increased crystallinities, suggest that the added PS in the PCDTBT:PCBM BHJ induces the *nucleation* of crystalline PCDTBT and PCBM domains.

The increasing crystallinities of both PCDTBT and PCBM phases in the PCDTBT:PCBM BHJ blend film by the addition of high MW PS are largely consistent with the observed trend of enhanced hole and electron mobilities in the BHJ layer with increasing PS MW, except that there is a more conspicuous enhancement of hole mobility than that of electron (Figure 2b). We interpret that the more enhanced hole mobility in the PCDTBT:PCBM blend by the

addition of PS is caused by the fact that the hole-conducting PCDTBT phase constitutes a significantly minor volume fraction compared with PCBM due to the large asymmetric blend ratio (i.e., PCDTBT:PCBM = 1:4 by wt.); this should cause the hole transport through the minor PCDTBT network to be more responsive to the structural improvement in PCDTBT domains than the electron transport through the major PCBM phase to the structural change in PCBM domains. It is noted that the hole transport in polymer phase in polymer:PCBM BHJ can be also improved by the change in polymer lamellar orientation with respect to the substrate surface, especially when the fraction of face-on lamellar stacking (i.e., π-π stacking) increases along the substrate plane normal direction.[22] The π-π stacked PCDTBT polymer backbones are known to be featured by the scattering peak located at q = ~1.36 $Å^{-1}$ in the GIWAXS data,[20] but our measured data show that the same q region is dominated by the isotropic scattering ring originating from the major PCBM, thus making the delineation and identification of PCDTBT π-π stacking peak and its potential redistribution along the plane normal direction difficult.[19c]

2.3. Effects of Polymer Interfacial Tension

2.3.1. Dependence of Interfacial Tension on PS MW

It has been shown that the nucleation of crystalline polymer phases could be enhanced by the presence of another polymer phase, whose origins were postulated to be related with the interfacial tension.[23] Here, we investigate whether this relationship is also applicable to the PCDTBT:PCBM BHJ blend with a minor addition of PS additive, wherein the GIWAXS data showed the overall enhanced crystallinity of PCDTBT phase for increasing MW of amorphous polymer additive, PS. Specifically, we examine if the increasing PS MW enhances the interfacial tension between PCDTBT and PS. In order to determine the interfacial tension of the two polymer phases, we use the nanoscale contact angle goniometry that enables the

measurement of the contact angle between PCDTBT and PS. The interfacial tension between the two polymers can be then determined via the Young's equation:[24]

$$\gamma_{pcdtbt} = \gamma_{ps} \cos\theta + \gamma_{inter} \quad (1)$$

, where γ_{pcdtbt} and $\gamma_{ps}$are, respectively, the surface tensions of PCDTBT and PS, γ_{inter} is the interfacial tension, and θ is Young's contact angle between PCDTBT and PS. γ_{pcdtbt} and γ_{ps}were first measured as a function of temperature using the two-liquid (water and diiodomethane) contact angle method,[25] where the surface tension of a given polymer can be computed by using the measured θ of polar (i.e., water) and non-polar (i.e., diiodomethane) liquids on the polymer thin film. γ_{pcdtbt} and γ_{ps} for varying PS MW (from 50K to 7M Da) were determined at five different temperature points (between 20 °C and ~50 °C) and linearly extrapolated to higher temperatures as shown in **Figure 6**a. Consistent to the typical polymer behavior, both γ_{pcdtbt} and γ_{ps} decrease for higher temperatures. Initially at low temperature, PS of all MWs exhibited higher γ_{ps} than γ_{pcdtbt}, but with increasing temperature, γ_{pcdtbt} became larger than γ_{ps} due to its lower temperature coefficient. Nevertheless, the overall difference between γ_{pcdtbt} and γ_{ps} is small (within ~10 %), making θ between the two polymers the primary factor that determines γ_{inter} between PS and PCDTBT. To measure θ between PCDTBT and PS of varying MW, the PS-PCDTBT bilayer thin film sample was subjected to a thermal annealing under vacuum at 150 °C, the identical temperature point at which PS-added PCDTBT:PCBM solar cells were annealed, for 72 h to achieve the dewetting (i.e., formation of droplets) of PS. Subsequently, the equilibrium θ between the two phases was measured ex situ by atomic force microscopy (AFM) after quickly cooling down the sample to room temperature (see the Experimental Section for more details).

As shown in Figure 6b (upper panel), θ of PS droplets on the PCDTBT thin film *increases* for a larger PS MW and eventually reaches a plateau for MW > 2M Da. This

increasing θ already qualitatively confirms the increasing γ_{inter} between PS and PCDTBT for a higher MW PS, being able to explain the enhanced PCDTBT crystallinity in the PCDTBT:PCBM BHJ blend with increasing PS MW. We further computed actual γ_{inter} values via Equation (1) by using the measured θ and the γ_{pcdtbt} and γ_{ps} values obtained at 150 °C in Figure 6a. It is found that γ_{inter} has an asymptotic MW-dependent increase similar to that of θ: Initially, γ_{inter} is 1.19×10^{-3} N/m at PS MW = 50k Da, increases for a larger PS MW, and finally saturates at ~3.55×10^{-3} N/m for MW > 2M Da (Figure 6b lower panel). Significantly, it is recognized that the PCE and charge mobilities (particularly, for hole) of PS-added PCDTBT:PCBM BHJ solar cells show the identical asymptotic increase with respect to PS MW as discussed earlier (Figure 2b), augmenting the notion of direct correlation between γ_{inter} and device photovoltaic performance via the phase crystallinity. Fundamentally, γ_{inter} is associated with the degree of immiscibility of two polymers via its general relationship with the Flory-Huggins parameter, χ, and, subsequently, the interfacial width, W, as described by the following equations:[26]

$$\gamma_{inter} = a\rho k_B T\sqrt{\frac{\chi}{6}} \quad (2)$$

$$W = \frac{2a}{\sqrt{6\chi}} \quad (3)$$

, where a is the effective length per monomer unit (~7 Å), ρ is the monomer density (~$10^{-2} \times N_A$ (Avogadro's number) units/cm^3), k_B is the Boltzmann constant, and T is the temperature. We find that there is a near ten-fold increase in χ between PCDTBT and PS as PS MW increases from 50k Da to >2M Da with corresponding W decreasing from ~19 Å to below 7 Å (Figure 6c and Table 3), highlighting the increased immiscibility between PCDTBT and PS for a high PS MW. These observations strongly support the critical roles of γ_{inter} between PS and PCDTBT in inducing the nucleation of crystalline domains in the PCDTBT:PCBM BHJ blend and eventually enhancing its solar cell performance.

2.3.2. Effects of PS MW on the Vertical Composition Profile in PCDTBT:PCBM BHJ Blends

We also find the high χ between PCDTBT and high MW PS drives the redistribution of PS to near the top surface of PCDTBT:PCBM BHJ blend layer, ultimately preventing the surface segregation of PCBM domains, which is undesirable for the hole collection in the inverted solar cell device structure. To determine the vertical compositional profile of the blend layer, we employed the time-of-flight secondary ion mass spectrometry (TOF-SIMS) and investigated the film composition as a function of depth. Deuterated-PS (dPS) was used as the additive in the PCDTBT:PCBM BHJ blend because of the excellent sensitivity of TOF-SIMS for detecting ^{2}H. **Figure 7**a shows the obtained depth-profiles of dPS volume fraction (f_{dPS}) in the PCDTBT:PCBM blend film having 2.5 wt.% of dPS additive with three different MWs (50k Da, 1M Da, and 2M Da). For the low MW (50k Da), dPS is relatively evenly distributed (at f_{dPS} <3 %) across the whole blend layer thickness except for a minor segregation near the bottom. However, a more visible redistribution of dPS toward the top and bottom of the BHJ blend layer is observed at MW = 1M Da, with the corresponding maximum local f_{dPS} increasing over 3 %. At the high MW (2M Da) over which we observed the most enhanced device PCE, there is a conspicuous concentration of dPS toward the top surface of blend layer, with nearly all dPS now being distributed within the top ~40 nm of blend layer and its local maximum f_{dPS} reaching up to ~8 %. This dPS concentration (i.e., segregation) at the upper portion of blend film is consistent to the GIWAXS data that showed a more significant increase in phase crystallinities for both PCDTBT and PCBM near the surface by the addition of high MW PS in the PCDTBT:PCBM blend film, considering that the high MW PS with high interfacial tension can enhance the nucleation of crystalline domains of the two phases.

We further discover that the redistribution of dPS also directly influences the vertical compositional profile of PCBM in the blend layer, preventing PCBM from majorly segregating near the top portion of PCDTBT:PCBM BHJ blend film. Figure 7b shows the TOF-SIMS depth-profiles of PCBM volume fraction (f_{PCBM}) in the PCDTBT:PCBM blend

film with different PS MWs, identified by the ^{16}O signal originating from PCBM. In the control blend film without dPS, f_{PCBM} is locally elevated within the top 30 nm of blend film, with the maximum f_{PCBM} reaching over 95 % at ~15 nm depth and f_{PCBM} = ~75 % at the very top of film. Driven by the lower surface tension of small molecular PCBM than polymers, PCBM naturally tends to segregate at the upper portion of polymer:PCBM BHJ blend film.[8] With 50k Da dPS, the aggregation of PCBM near the upper portion of blend layer is maintained with its maximum f_{PCBM} still over 95 % at ~5 nm depth and f_{PCBM} even reaching ~91 % at the top film surface. However, when 1M Da PS is introduced in the blend film, f_{PCBM} decreases below 90 % within the top portion of blend with the surface f_{PCBM} decreasing to ~73 %. Ultimately, when 2M Da dPS is added into the blend, the PCBM desegregation from the top portion of blend film continues with the surface f_{PCBM} now greatly reduced to ~43 %, making the local PCDTBT:PCBM blend ratio much more balanced than before. We expect this balanced blend ratio caused by the desegregation of PCBM from the top portion of PCDTBT:PCBM blend film by the addition of high MW PS is another important factor that contributed to the enhancement of solar cell performance as it helps the efficient hole extraction by the top anode of inverted device structure.

Finally, the PS-interfacial-tension-driven increase in phase crystallinities near the surface of PCDBT:PCBM BHJ blend thin films was further confirmed by the AFM topography and lateral force (i.e., surface friction) imaging conducted as a function of the MW of PS additives (**Figure 8**). Clearly, the surface roughness observed in the topographic imaging increases markedly as the PS MW becomes larger than 1M Da (Figure 8a-d upper panels), seemingly consistent to the notion of increased phase crystallinities near the surface. The surface friction imaging, however, shows that the control PCDTBT:PCBM blend film without PS and the blend film with low-MW (50k Da) PS both feature a negligible spatial variation (Figure 8a,b lower panels) unlike their topography counterparts, suggesting that despite some roughness, the surface of BHJ film without PS or with low-MW PS is likely covered with amorphous

phases without much crystallintiy. It is when the PS MW is larger than 1M Da, the spatial variation in surface friction becomes visibly noticeable and comparable to that of the surface roughness (Figure 8c-e). Given that crystalline and amorphous domains generally exert significantly different mechanical stiffness, the observed large spatial variation in surface friction on the PCDTBT:PCBM BHJ blend with high-MW PS confirms the nucleation of crystalline domains near the surface driven by the segregation of PS toward the upper portion of blend film.

2.4. Structural Model for PCDTBT:PCBM BHJ Blend with Tertiary PS Additives

Based on the structural characteristics identified by the GIWAXS, interfacial tension, and TOF-SIMS analyses, the evolution of the internal structure of PCDTBT:PCBM BHJ blend films with respect to increasing PS additive MW can be depicted by the schematic internal structures provided in **Figure 9**, explaining the corresponding device charge transport and photovoltaic performance. Initially, when no PS additives are added to the PCDTBT:PCBM blend, there is a natural tendency for PCBM, as a small molecule with lower surface tension than polymers, to segregate near the top surface of the blend film (Figure 9a). For the inverted device structure in which holes must be extracted through the anode located atop, this PCBM segregation at the upper portion of blend film limits the efficient charge extraction, therefore limiting the device J_{sc}, FF, and finally PCE, the parameters directly impacted by the charge transport efficiency. The PCBM segregation issue is more exacerbated by the fact that the low immiscibility between PCDTBT (and most low bandgap polymers) and PCBM necessitates the incorporation of a larger amount of PCBM relative to PCDTBT in the blend (PCDTBT:PCBM = 1:4 by wt.) for a proper phase separation, which leads to a more decreased amount of PCDTBT near the top surface, further reducing hole extraction pathways.

When the low-to-intermediate MW (e.g., 50k – 1M Da) PS additive is mixed with PCDTBT:PCBM blend (Figure 9b), its interfacial tension with PCDTBT starts driving the

distribution of PS toward the upper portion of blend film and the subsequent displacement of PCBM away from the interfacial area between the blend-film and top electrode. The distributed PS also starts inducing the nucleation of both PCDTBT and PCBM crystalline domains, increasing the phase crystallinities within the bulk of blend film and near the top surface, but more so for the latter as PS is becoming more concentrated in that region. These structural changes start positively influencing the device photovoltaic performance, but the interfacial tension imparted by the PS of low-to-intermediate MW is yet insufficient to fully exploit the structural improvement attainable by the PS additive.

It is only when the high MW (>2M Da) PS is added to PCDTBT:PCBM blend (Figure 9c), the maximized interfacial energy between the two homopolymer components, PCDTBT and PS, can result in the most enhanced charge carrier collection and, therefore, device photovoltaic performance by driving the redistribution of nearly all added PS to the upper ~30 nm portion of blend film, rendering the surface PCBM volume fraction being reduced below 50 % to result in a balanced PCDTBT:PCBM local blend ratio, and further induce the nucleation of crystalline domains of PCDTBT and PCBM, increasing the overall phase crystallinities within the BHJ blend film. Along with the dramatic vertical compositional profile change, the increased phase crystallinities by the addition of high MW PS facilitates a more efficient transport of photogenerated charge carriers, and particularly to a greater degree for holes because their conduction through the minor phase PCDTBT polymer network within the initial, unmodified PCDTBT:PCBM BHJ blend film is much less efficient compared with that of electrons through the major phase PCBM due to the necessary, highly asymmetric blend ratio. Overall, these new internal BHJ morphologies regulated by the high MW PS additive enable the balanced charge transport within the bulk of BHJ blend film as well as the improved hole collection by the top anode, ultimately leading to the enhanced device photovoltaic performance of inverted PCDTBT:PCBM BHJ solar cells.

3. Conclusion

We have shown that the addition of small amount (2.5 wt.%) of high MW (>2M Da) PS to the low bandgap polymer BHJ blend consisting of PCDTBT and PCBM could significantly enhance the hole mobility through the polymer network in the BHJ blend (by ~500 %), ultimately resulting in the improved device photovoltaic performance of PCDTBT:PCBM inverted solar cells (PCE improvement by ~20%). The investigation of blend internal structure by GIWAXS and TOF-SIMS confirmed that the observed enhancements were driven by the redistribution of added PS additive toward the upper portion of BHJ blend film, which not only reduced the segregation of PCBM phase near the top anode, a natural phenomenon generally occurring in the polymer:fullerne BHJ and undesirable for the efficient operation of inverted-structure BHJ solar cells, but also significantly increased the phase crystallinities within the BHJ blend film. From the PS-MW-dependent interfacial tension measurement and associated analysis, we found that the interfacial tension between PCDTBT and PS increased nearly ten-fold as MW increased from 50k Da to 2M Da, fundamentally responsible for the identified evolution of the internal structure of PCDTBT:PCBM BHJ blend film. Given that the surface segregation of PCBM and the poor hole transport through polymer phases are common issues in the low bandgap polymer:fullerene BHJ blend due to its highly fullerene-dominant asymmetric blend ratio required for high photovoltaic performances, the results show that high-MW tertiary polymers can be effective additives for the low bandgap polymer BHJ solar cell, regulating the internal BHJ morphology for efficient charge transport and improving device photovoltaic performances. We also expect that other macromolecular BHJ components (such as new non-fullerene acceptors) with interfacial energies comparable to those of low-bandgap polymer donors can be similarly influenced by the demonstrated high-MW polymer additive approach. The revealed correlation between the polymer interfacial tension, vertical composition redistribution in the BHJ blend, and phase

crystallinity also provides useful general guidelines for developing high-performance ternary polymer solar cells.

4. Experimental Section

Materials: PCDTBT was purchased from 1-Material. PCBM was provided by SES Research. Chlorobenzene is obtained from Sigma-Aldrich. PS with various MWs was purchased from Polymer Source. All materials are used without further purification.

Device fabrication: All the device fabrication procedures were performed in air unless noted otherwise. ITO-coated glass substrates were treated with ultraviolet (UV)-ozone for 10 min. TiO_2 precursor solution was synthesized according to a previous report.[27] A 30 nm thick TiO_2 layer was spin-cast onto the ITO-glass substrate at 3000 rpm for 20 s and was baked at 400 °C for 2 h on a hot plate. Chlorobenzene solution composed of PS:PCDTBT:PCBM (2.5:19.5:78 by wt.) was spin-cast at 3000 rpm for 45 s on top of TiO_2 layer. The typical film thickness of active layer is around 100 nm. The samples were then annealed in vacuum oven (~100 mTorr) at 150 °C for 10 min. Finally, the devices were completed by thermal evaporation of 8 nm thick MoO_3 and 100 nm thick Ag electrode (Kurt J. Lesker PVD 75).

Photovoltaic characterization: The photovoltaic performance of fabricated solar cells was tested by a modified probe station equipped with a 150 W solar simulator (Oriel) with an air mass 1.5 global (AM1.5G) filter and precision semiconductor parameter analyzer (Agilent). The light intensity was calibrated to 100 $mWcm^{-2}$ (1 Sun) by a calibrated Si solar cell (Oriel). 3-5 devices were measured for each condition for statistics.

Space charge limited current (SCLC) mobility measurement: The hole-only and electron-only diodes were fabricated for the SCLC mobility measurement. The device geometry is similar to that of a solar cell, except that TiO_2 was replaced by PEDOT:PSS for hole-only diodes while MoO_3/Ag was substituted by Al for electron-only diodes. Measured device J–V

characteristics were fitted to the Mott–Gurney equation:[18] $J = 9\varepsilon_r\varepsilon_0\mu V^2/(8L^3)$, where ε_r is the relative dielectric constant, ε_0 the vacuum permittivity, μ the mobility, and L the active layer thickness.

Interfacial tension measurement: The interfacial tension between PCDTBT and PS was determined via the contact angle goniometry and Young's equation[24a] that correlates the surface tensions of individual polymers with their contact angle and interfacial tension as more details are provided in the Discussion section. First, the surface tensions of PCDTBT and PS were measured by as a function of temperature in an enclosed sample stage on a hot plate via the two-liquid (water and diiodomethane) contact angle method.[25] Then, the interfacial contact angle between PS and PCDTBT was measured by using bilayer thin films consisting of PS layer (~20 nm thick) on top of PCDTBT layer (~45 nm thick) on a Si substrate, to finally determine the interfacial surface tension. To prepare the bilayer film, Si substrates (2×2 cm^2) were first treated with the modified Shiraki technique:[28] The substrates were immersed in a H_2O:H_2O_2:H_2SO_4 (3:1:1 by vol.) solution for 15 min at 80 °C, rinsed in deionized water, and immersed in a diluted hydrofluoric acid solution (H_2O:HF = 15:1 by vol.) for 20 s at room temperature to create a hydrophobic surface. The PCDTBT solution (1 wt.% in chlorobenzene) was spin-cast onto the HF-treated Si substrate at 2000 rpm for 45 s. The samples were then annealed at 150 °C in a vacuum (100 mTorr) for 5 h to remove the residual solvent and relax strains induced by the spin-casting process. Then, a PS solution (0.6 wt.% in chlorobenzene) was spin-cast (2000 rpm for 45 s) onto a separate Si substrate, and the PS film was carefully floated off in deionized water onto the PCDTBT-coated Si substrate. The resultant bilayer films were then dried in a vacuum oven at 40 °C for 12 h. To measure the interfacial contact angle, the bilayer film was annealed at 150 °C under vacuum for 72 h to achieve the dewetting of PS film into droplets (cf., T_g of PS = ~100 °C), whose contact angles were directly measured by AFM (Bruker) and analyzed by the VEECO/DI contact angle

software.[29] The temperature of polymer thin film surface was all measured by a pyrometer during the experiment.

GIWAXS measurement: The internal structure of PCDTBT:PCBM BHJ blend films were investigated by 2D GIWAXS carried out at the 8-ID-E beamline (λ = 0.11363 nm and E = 10.91 keV) at the Advanced Photon Source (APS), Argonne National Laboratory. Two different GIWAXS modes, surface and film modes, were used for the experiment. The surface mode uses α (incident angle) just below α_c (critical angle for the total external reflection on PCDTBT, 0.13°), such that the electric field intensity decays exponentially into the film, rendering the X-ray scattering intensity being dominated by ~10 nm upper portion of BHJ blend films. On the other hand, under the film mode, the X-ray penetration depth exceeds the BHJ blend film thickness, providing the structural information averaged over the entire film thickness. All samples were measured at room temperature under vacuum (~200 mTorr). 1D line cuts were obtained by integrating the X-ray scattering intensity in 2D GWAXS data for the ω range from 135 ° to 145 °.

TOF-SIMS measurement: The vertical compositional profiles of BHJ blend films on SiO_2/Si substrates were obtained with a PHI TRIFT V nanoTOF-SIMS at the City University of New York Advanced Science Research Center. A 2 kV argon beam at ~45 nA beam current was rastered across a 400 μm × 400 μm area, of which only the middle 10 % was analyzed for composition by collecting negative secondary ions. The films were prepared by spin-casting blend solutions on SiO_2/Si substrates using the identical processing parameters used for fabricating solar cells. The signal for PCBM originates from ^{16}O while the ^{2}H signal represents dPS. Si and carbon signals were collected for determining the end point of film. A typical measured depth profile is provided in Figure S4, where the small oxygen peak with width of ~3 nm at the depth of ~90 nm represents the native SiO_2 layer underneath the BHJ blend film.

AFM topography and surface friction imaging: The topography and spatial variation in surface friction on PCDTBT:PCBM BHJ thin films were characterized as a function of PS additive MW by the contact-mode AFM (Bruker Dimension Icon).

Supporting Information

Supporting Information is available from the Wiley Online Library or from the author.

Acknowledgements

We gratefully acknowledge the financial support by NSF-1344267 INSPIRE program. This research was in part carried out at the Center for Functional Nanomaterials (CFN) of Brookhaven National Laboratory, which is supported by the U.S. Department of Energy, Office of Basic Energy Sciences, under contract no. DE-SC0012704. We also acknowledge the access to the ThINC facility at the Advanced Energy Center, Stony Brook University and the facility at Advanced Science Research Center, the City University of New York.

Received: ((will be filled in by the editorial staff))
Revised: ((will be filled in by the editorial staff))
Published online: ((will be filled in by the editorial staff))

References

[1] a) C. J. Brabec, N. S. Sariciftci, J. C. Hummelen, *Adv. Funct. Mater.* 2001, 11, 15; b) F. C. Krebs, *Org. Electron.* 2009, 10, 761; c) J. J. van Franeker, M. Turbiez, W. W. Li, M. M. Wienk, R. A. J. Janssen, *Nat. Commun.* 2015, 6, 6229; d) M. M. Voigt, R. C. I. Mackenzie, C. P. Yau, P. Atienzar, J. Dane, P. E. Keivanidis, D. D. C. Bradley, J. Nelson, *Sol. Energy Mater. Sol. Cells* 2011, 95, 731.

[2] a) T. Ameri, G. Dennler, C. Waldauf, H. Azimi, A. Seemann, K. Forberich, J. Hauch, M. Scharber, K. Hingerl, C. J. Brabec, *Adv. Funct. Mater.* 2010, 20, 1592; b) S. K. Hau, H.-L. Yip, A. K. Y. Jen, *Polym. Rev.* 2010, 50, 474; c) G. Li, C. W. Chu, V. Shrotriya, J. Huang, Y. Yang, *Appl. Phys. Lett.* 2006, 88, 253503; d) C. Waldauf, M. Morana, P. Denk, P. Schilinsky, K. Coakley, S. A. Choulis, C. J. Brabec, *Appl. Phys. Lett.* 2006, 89, 233517; e) Y. Sun, J. H. Seo, C. J. Takacs, J. Seifter, A. J. Heeger, *Adv. Mater.* 2011, 23, 1679; f) T. Yang, W. Cai, D. Qin, E. Wang, L. Lan, X. Gong, J. Peng, Y. Cao, *J. Phys. Chem. C* 2010, 114, 6849; g) X. Wei, P. Panindre, Q. Zhang, Y.-A. Song, *ACS Sensors* 2016, 1, 862.

[3] a) C.-H. Hsieh, Y.-J. Cheng, P.-J. Li, C.-H. Chen, M. Dubosc, R.-M. Liang, C.-S. Hsu, *J. Am. Chem. Soc.* 2010, 132, 4887; b) J. S. Park, B. R. Lee, J. M. Lee, J. S. Kim, S. O. Kim, M. H. Song, *Appl. Phys. Lett.* 2010, 96, 243306.

[4] a) C. Pan, H. Li, B. Akgun, S. K. Satijia, Y. Zhu, D. Xu, J. Ortiz, D. Gersappe, M. H. Rafailovich, *Macromolecules* 2013, 46, 1812; b) Z. Yang, M. Moffa, Y. Liu, H. Li, L. Persano, A. Camposeo, R. Saija, M. A. Iatì, O. M. Maragò, D. Pisignano, C.-Y. Nam, E. Zussman, M. Rafailovich, *J. Phys. Chem. C* 2018, 122, 3058.

[5] N. M. Bedford, M. B. Dickerson, L. F. Drummy, H. Koerner, K. M. Singh, M. C. Vasudev, M. F. Durstock, R. R. Naik, A. J. Steckl, *Adv. Energy Mater.* 2012, 2, 1136.

[6] a) L.-M. Chen, Z. Hong, G. Li, Y. Yang, *Adv. Mater.* 2009, 21, 1434; b) B. A. Collins, E. Gann, L. Guignard, X. He, C. R. McNeill, H. Ade, *J. Phys. Chem. Lett.* 2010, 1, 3160; c) M. Kim, J. Lee, S. B. Jo, D. H. Sin, H. Ko, H. Lee, S. G. Lee, K. Cho, *J. Mater. Chem. A* 2016, 4, 15522; d) F. Liu, Y. Gu, X. Shen, S. Ferdous, H.-W. Wang, T. P. Russell, *Prog. Polym. Sci.* 2013, 38, 1990; e) M. C. Scharber, N. S. Sariciftci, *Prog. Polym. Sci.* 2013, 38, 1929; f) Q. Zhang, A. Prabhu, A. San, J. F. Al-Sharab, K. Levon, *Biosens. Bioelectron.* 2015, 72, 100; g) Y. Zhou, J. Huang, W. Sun, Y. Ju, P. Yang, L. Ding, Z.-R. Chen, J. A. Kornfield, *ACS Appl. Mater. Interfaces* 2017, 9, 4177.

[7] a) J. Huang, J. H. Carpenter, C.-Z. Li, J.-S. Yu, H. Ade, A. K. Y. Jen, *Adv. Mater.* 2016, 28, 967; b) B. J. Tremolet de Villers, R. C. I. MacKenzie, J. J. Jasieniak, N. D. Treat, M. L. Chabinyc, *Adv. Energy Mater.* 2014, 4, 1301290; c) Z. Xiao, Y. Yuan, B. Yang, J. VanDerslice, J. Chen, O. Dyck, G. Duscher, J. Huang, *Adv. Mater.* 2014, 26, 3068; d) M. Kaisti, Q. Zhang, K. Levon, *Sens. Actuators, B* 2017, 241, 321; e) Q. Zhang, A. Khajo, T. Sai, I. de Albuquerque, R. S. Magliozzo, K. Levon, *J. Phys. Chem. A* 2012, 116, 7629.

[8] H. Wang, E. D. Gomez, J. Kim, Z. Guan, C. Jaye, D. A. Fischer, A. Kahn, Y.-L. Loo, *Chem. Mater.* 2011, 23, 2020.

[9] H. Li, Z. Yang, C. Pan, N. Jiang, S. K. Satija, D. Xu, D. Gersappe, C.-Y. Nam, M. H. Rafailovich, *Nanoscale* 2017, 9, 11511.

[10] Z. Sun, K. Xiao, J. K. Keum, X. Yu, K. Hong, J. Browning, I. N. Ivanov, J. Chen, J. Alonzo, D. Li, B. G. Sumpter, E. A. Payzant, C. M. Rouleau, D. B. Geohegan, *Adv. Mater.* 2011, 23, 5529.

[11] Y. H. Huh, B. Park, *Opt. Express* 2013, 21, A146.

[12] a) Z. Xiao, X. Jia, L. Ding, *Sci. Bull.* 2017, 62, 1562; b) Z. Xiao, X. Jia, D. Li, S. Wang, X. Geng, F. Liu, J. Chen, S. Yang, T. P. Russell, L. Ding, *Sci. Bull.* 2017, 62, 1494.

[13] H. Li, Z. Xiao, L. Ding, J. Wang, *Sci. Bull.* 2018, 63, 340.

[14] T. Y. Chu, S. Alem, P. G. Verly, S. Wakim, J. P. Lu, Y. Tao, S. Beaupre, M. Leclerc, F. Belanger, D. Desilets, S. Rodman, D. Waller, R. Gaudiana, *Appl. Phys. Lett.* 2009, 95, 044906.

[15] a) S. H. Anastasiadis, I. Gancarz, J. T. Koberstein, *Macromolecules* 1988, 21, 2980; b) J. Li, X. Feng, B. Liu, Y. Yu, L. Sun, T. Liu, Y. Wang, J. Ding, X. Chen, *Acta Biomaterialia* 2017, 61, 21; c) M. Si, T. Araki, H. Ade, A. L. D. Kilcoyne, R. Fisher, J. C. Sokolov, M. H. Rafailovich, *Macromolecules* 2006, 39, 4793.

[16] Y. Huang, W. Wen, S. Mukherjee, H. Ade, E. J. Kramer, G. C. Bazan, *Adv. Mater.* 2014, 26, 4168.

[17] V. Vohra, M. Campoy-Quiles, M. Garriga, H. Murata, *J. Mater. Chem.* 2012, 22, 20017.

[18] M. A. Lampert, P. Mark, *Current injection in solids*, Academic Press, New York, 1970.

[19] a) W. Yin, M. Dadmun, *ACS Nano* 2011, 5, 4756; b) A. J. Pearson, T. Wang, A. D. F. Dunbar, H. Yi, D. C. Watters, D. M. Coles, P. A. Staniec, A. Iraqi, R. A. L. Jones, D. G. Lidzey, *Adv. Funct. Mater.* 2014, 24, 659; c) X. H. Lu, H. Hlaing, D. S. Germack, J. Peet, W. H. Jo, D. Andrienko, K. Kremer, B. M. Ocko, *Nat. Commun.* 2012, 3, 795.

[20] P. A. Staniec, A. J. Parnell, A. D. F. Dunbar, H. Yi, A. J. Pearson, T. Wang, P. E. Hopkinson, C. Kinane, R. M. Dalgliesh, A. M. Donald, A. J. Ryan, A. Iraqi, R. A. L. Jones, D. G. Lidzey, *Adv. Energy Mater.* 2011, 1, 499.

[21] M.-Y. Chiu, U. S. Jeng, C.-H. Su, K. S. Liang, K.-H. Wei, *Adv. Mater.* 2008, 20, 2573.

[22] T. Kim, J.-H. Kim, T. E. Kang, C. Lee, H. Kang, M. Shin, C. Wang, B. Ma, U. Jeong, T.-S. Kim, B. J. Kim, *Nat. Commun.* 2015, 6, 8547.

[23] a) S. T. Milner, *Soft Matter* 2011, 7, 2909; b) R. Dell'Erba, G. Groeninckx, G. Maglio, M. Malinconico, A. Migliozzi, *Polymer* 2001, 42, 7831.

[24] a) S. Wu, *J. Polym. Sci., Part C: Polym. Symp.* 1971, 34, 19; b) Y. Guo, Y. Xue, X. Zuo, L. Zhang, Z. Yang, Y. Zhou, C. Marmorat, S. He, M. Rafailovich, *Polym. Degrad. Stab.* 2017, 144, 155.
[25] Y. Guo, S. He, K. Yang, Y. Xue, X. Zuo, Y. Yu, Y. Liu, C.-C. Chang, M. H. Rafailovich, *ACS Appl. Mater. Interfaces* 2016, 8, 17565.
[26] a) C. J. Clarke, A. Eisenberg, J. La Scala, M. H. Rafailovich, J. Sokolov, Z. Li, S. Qu, D. Nguyen, S. A. Schwarz, Y. Strzhemechny, B. B. Sauer, *Macromolecules* 1997, 30, 4184; b) E. Helfand, Y. Tagami, *J. Polym. Sci., Part B: Polym. Lett.* 1971, 9, 741.
[27] H. L. Xue, X. Z. Kong, Z. R. Liu, C. X. Liu, J. R. Zhou, W. Y. Chen, S. P. Ruan, Q. Xu, *Appl. Phys. Lett.* 2007, 90, 201118.
[28] A. Ishizaka, Y. Shiraki, *J. Electrochem. Soc.* 1986, 133, 666.
[29] a) S. Pack, T. Kashiwagi, C. Cao, C. S. Korach, M. Lewin, M. H. Rafailovich, *Macromolecules* 2010, 43, 5338; b) Y. Guo, K. Yang, X. Zuo, Y. Xue, C. Marmorat, Y. Liu, C.-C. Chang, M. H. Rafailovich, *Polymer* 2016, 83, 246; c) Y. Yu, Q. Zhang, J. Buscaglia, C.-C. Chang, Y. Liu, Z. Yang, Y. Guo, Y. Wang, K. Levon, M. Rafailovich, *Analyst* 2016, 141, 4424; d) Y. Yu, Q. Zhang, C.-C. Chang, Y. Liu, Z. Yang, Y. Guo, Y. Wang, D. K. Galanakis, K. Levon, M. Rafailovich, *Analyst* 2016, 141, 5607.

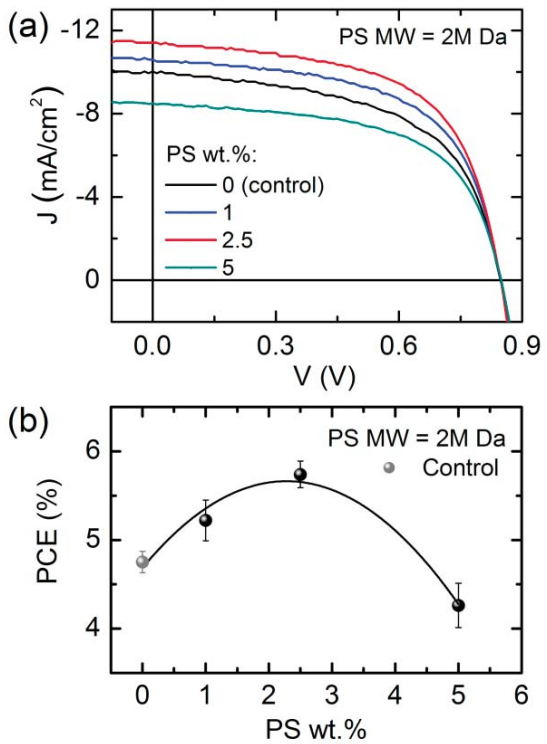

Figure 1. (a) Representative J-V characteristics of PCDTBT:PCBM BHJ solar cells having tertiary PS additives (MW = 2M Da) of various PS wt.%, measured under 1 Sun AM1.5G illumination condition. (b) Average PCE of PCDTBT:PCBM BHJ solar cells having tertiary PS additives (MW = 20M Da) as a function of PS wt.%.

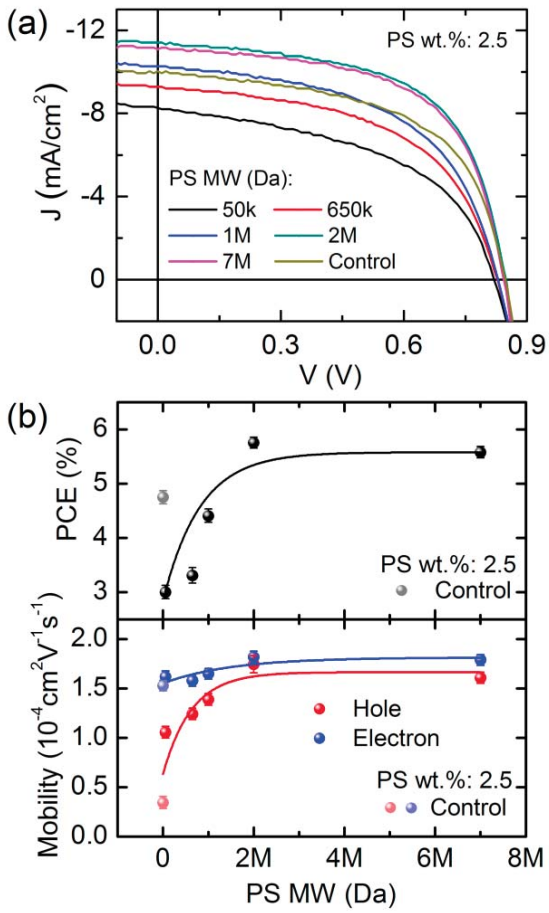

Figure 2. (a) Representative J-V characteristics of PCDTBT:PCBM BHJ solar cells having tertiary PS additives (concentration: 2.5 wt.%) of various MWs, measured under 1 Sun AM1.5G illumination condition. (b) Average PCE of PCDTBT:PCBM BHJ solar cells having tertiary PS additives (concentration: 2.5 wt.%) and corresponding charge mobilities as a function of PS MW. "Control" denotes the BHJ blend thin film without PS additive.

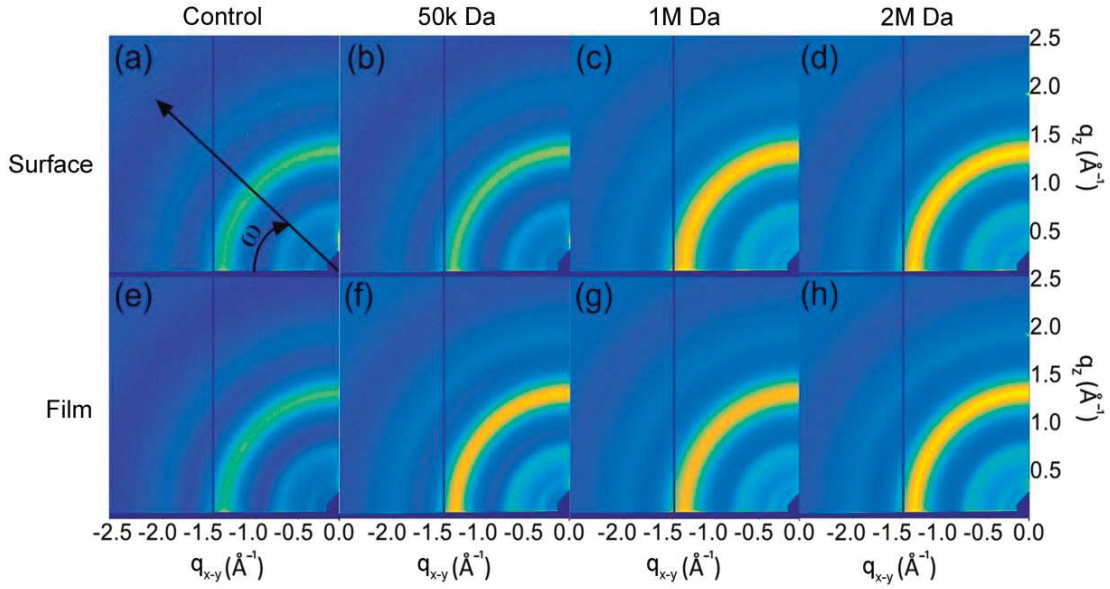

Figure 3. 2D GIWAXS intensity profiles measured by either surface or film mode from PCDTBT:PCBM BHJ blend thin films having tertiary PS additives of various MWs. "Control" denotes the BHJ blend thin film without PS additive.

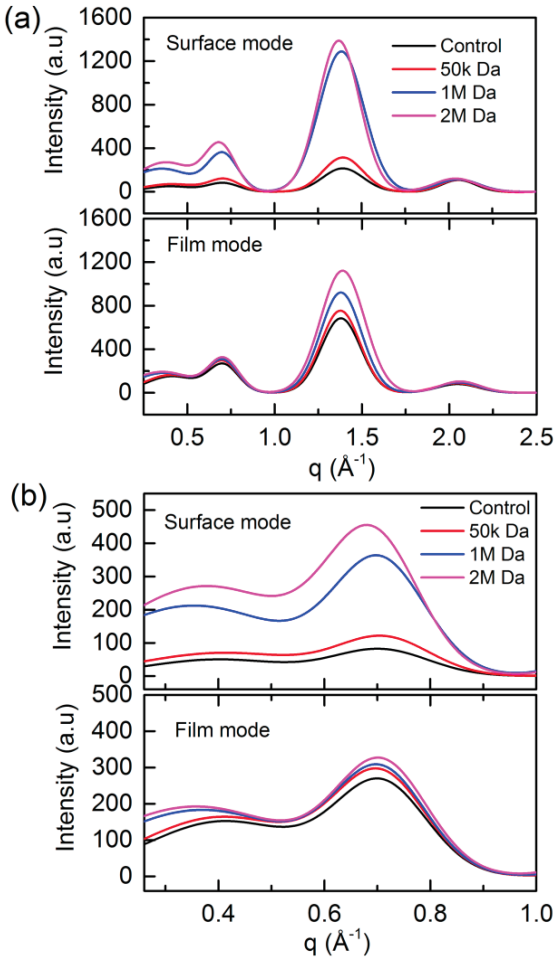

Figure 4. (a) 1D GIWAXS intensity profiles (i.e., line cuts obtained from Figure 3) measured by either surface or film mode from PCDTBT:PCBM BHJ blend thin films having tertiary PS additives of various MWs. "Control" denotes the control blend thin film without PS additive. (b) Magnified 1D GIWAXS intensity profiles for the q range < 1 Å^{-1}.

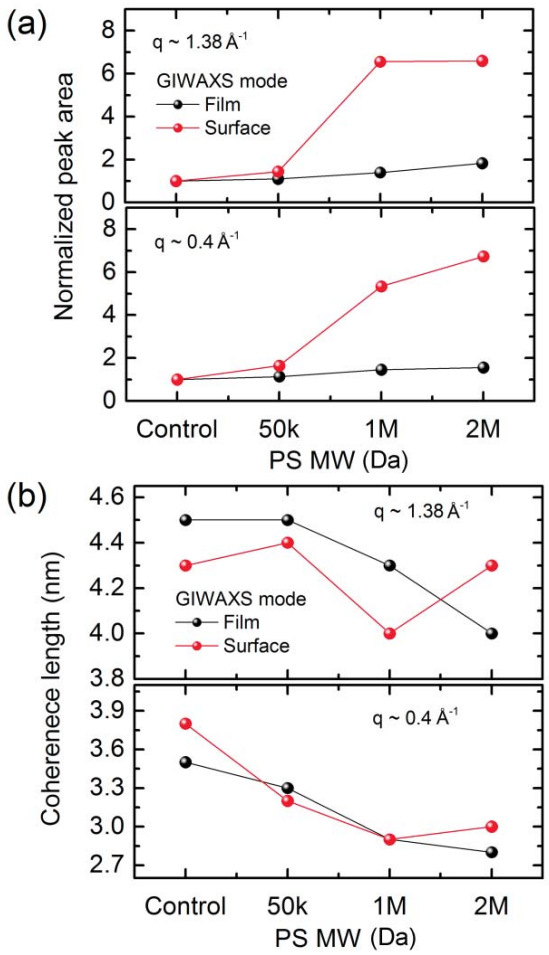

Figure 5. (a) Peak area (i.e., crystallinity) and (b) coherence length (i.e., crystalline domain size) of PCDTBT:PCBM BHJ blend thin films having tertiary PS additives as a function of PS MWs at q ~1.38 $Å^{-1}$ (corresponding to PCBM crystalline domains) and q ~ 0.4 $Å^{-1}$ (corresponding to PCDTBT lamellar stacking), measured by either film or surface mode. The values are determined by the deconvolution parameters obtained from the 1D GIWAXS intensity profiles in Figure 4. "Control" denotes the PCDTBT:PCBM BHJ blend thin film without PS additive. The peak areas are normalized by that of the control PCDTBT:PCBM BHJ blend thin film.

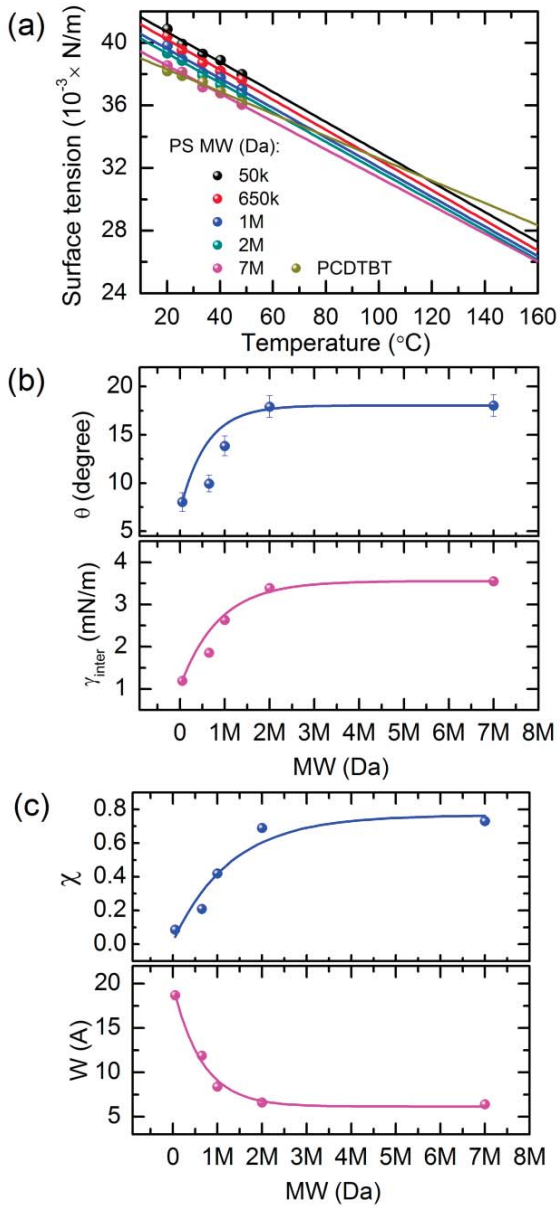

Figure 6. (a) Surface tensions of PS having various MWs and PCDTBT measured as a function of temperature. (b) Measured θ (contact angle) and corresponding γ_{inter} (interfacial tension) between PCDTBT and PS as a function of PS MW, and (c) further determined PS-MW-dependent, corresponding χ (Flory-Huggins parameter) and W (interfacial width) between the two polymers.

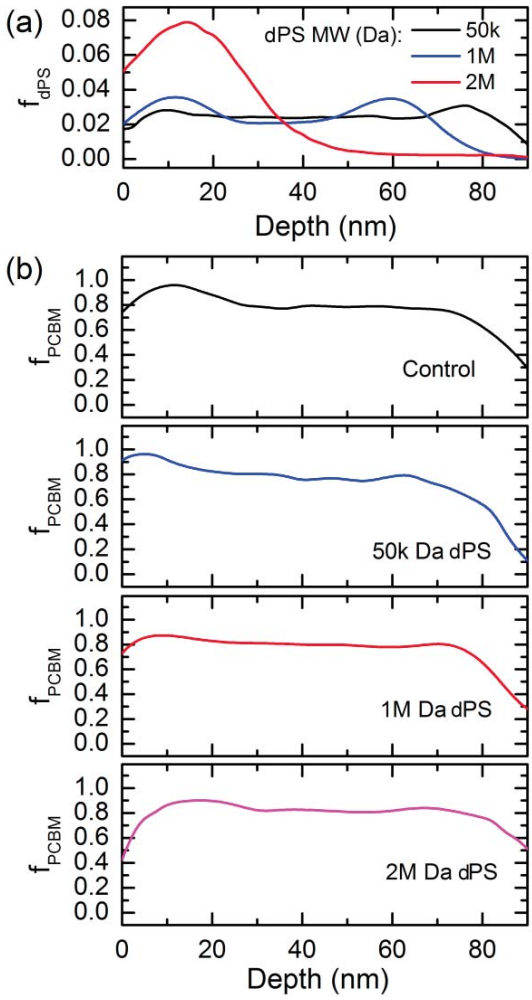

Figure 7. TOF-SIMS depth-profiles of: (a) f_{dPS} (dPS volume fraction) and (b) f_{PCBM} (PCBM volume fraction) in PCDTBT:PCBM BHJ blend thin films with tertiary dPS additives of various MWs. "Control" denotes the BHJ blend thin film without dPS additive.

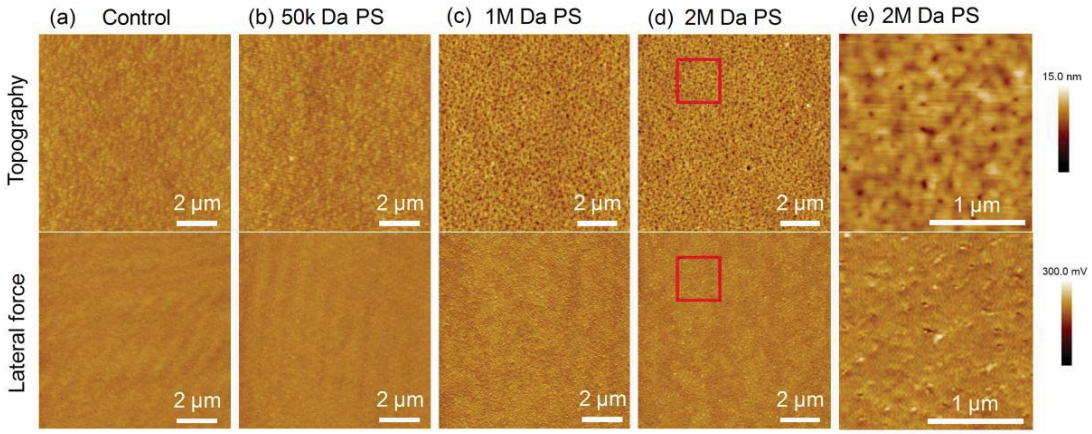

Figure 8. AFM topography and lateral force (surface friction) images obtained on PCDTBT:PCBM BHJ blend thin films with various PS MWs. (a) Control, (b) 50k Da, (c) 1M Da, and (d) 2M Da. (e) displays the magnified views of the red-framed areas in (d). "Control" denotes the BHJ blend thin film without PS additive.

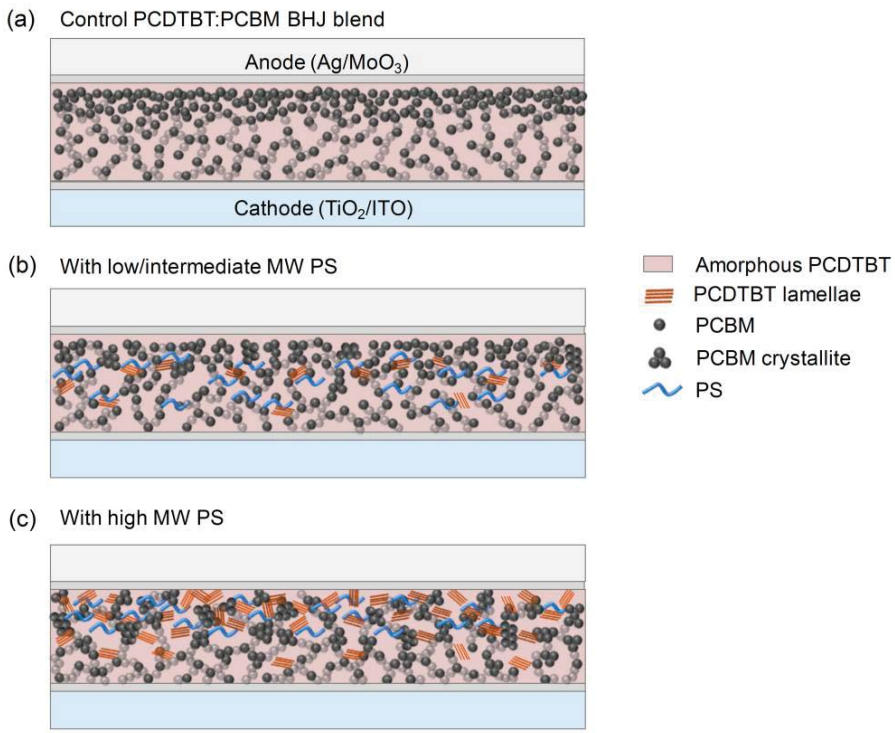

Figure 9. Schematic description of the PS-MW-dependent evolution of internal morphology in the PCDTBT:PCBM BHJ blend thin film with tertiary PS additives. (a) Control BHJ blend without PS additive. (b) With low-to-intermediate MW PS. (c) With high MW PS.

Table 1. Average device photovoltaic performance parameters of PCDTBT:PCBM BHJ solar cells having various concentrations of tertiary PS additives (MW = 2M Da)

PS wt.%	J_{sc} [mA/cm^2]	V_{oc} [V]	FF	PCE [%]
0 (control)	10.0 ± 0.3	0.84 ± 0.01	0.57 ± 0.02	4.8 ± 0.1
1	10.6 ± 0.5	0.84 ± 0.02	0.59 ± 0.03	5.2 ± 0.2
2.5	11.3 ± 0.4	0.85 ± 0.01	0.60 ± 0.02	5.7 ± 0.2
5	8.6 ± 0.3	0.84 ± 0.01	0.59 ± 0.02	4.3 ± 0.3

Table 2. Average device photovoltaic performance parameters of PCDTBT:PCBM BHJ solar cells having various MWs of tertiary PS additives (concentration: 2.5 wt.%) and their corresponding hole and electron mobilities (μ_h and μ_e, respectively)

PS MW [Da]	J_{sc} [mA/cm^2]	V_{oc} [V]	FF	PCE [%]	μ_h [×10^{-4} cm^2/V-s]	μ_e [×10^{-4} cm^2/V-s]
0[a)]	10.0 ± 0.3	0.84 ± 0.01	0.57 ± 0.02	4.8 ± 0.1	0.34 ± 0.06	1.53 ± 0.05
50k	8.4 ± 0.5	0.84± 0.02	0.48 ± 0.03	3.4 ± 0.3	1.05 ± 0.06	1.62 ± 0.06
650k	9.5 ± 0.4	0.82 ± 0.02	0.52 ± 0.03	4.0 ± 0.2	1.24 ± 0.06	1.58 ± 0.06
1M	10.0 ± 0.3	0.82 ± 0.01	0.55 ± 0.02	4.5 ± 0.1	1.38 ± 0.06	1.65 ± 0.06
2M	11.3 ± 0.4	0.85 ± 0.01	0.60 ± 0.02	5.7 ± 0.2	1.75 ± 0.09	1.82 ± 0.06
7M	11.3 ± 0.4	0.84 ± 0.02	0.59 ± 0.02	5.6 ± 0.2	1.61 ± 0.06	1.79 ± 0.05

[a)]Control sample without PS

Interfacial tension provided by high molecular weight polymer additives enhance the device photovoltaic performance of inverted low bandgap polymer:fullerene bulk heterojuction solar cells by increasing the crystallinities of photoactive phases and preventing the interfacial segregation of fullerenes near the hole-collecting anode.

Keyword: low bandgap polymer solar cells, ternary blends, polymer additives, interfacial tension, crystallinity

Z. Yang, H. Li, Y. Guo, Y. Zhou, X. Zuo, Y. Yu, J. Strzalka, C.-Y. Nam*, and M. H. Rafailovich*

Roles of Interfacial Tension in Regulating Internal Organization of Low Bandgap Polymer Bulk Heterojunction Solar Cells by Polymer Additives

ToC figure

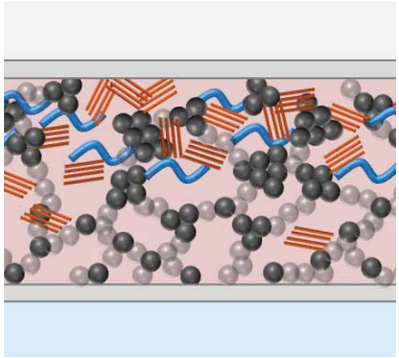

Supporting Information

Roles of Interfacial Tension in Regulating Internal Organization of Low Bandgap Polymer Bulk Heterojunction Solar Cells by Polymer Additives

Zhenhua Yang, Hongfei Li, Yichen Guo, YuchenZhou, XianghaoZuo, YingjieYu, Joseph Strzalka, Chang-Yong Nam, and Miriam H. Rafailovich**

Dr. Z. Yang, Dr. H. Li, Y. Guo, Y. Zhou, X. Zuo, Y. Yu, Prof. M. H. Rafailovich
Department of Materials Science and Chemical Engineering, Stony Brook University, Stony Brook, NY 11794, USA
E-mail: miriam.rafailovich@stonybrook.edu
Dr. C.-Y. Nam
Center for Functional Nanomaterials, Brookhaven National Laboratory, Upton, NY 11973, USA
E-mail: cynam@bnl.gov
Dr. J. Strzalka
X-ray Science Division, Argonne National Laboratory, Argonne, IL 60439, USA

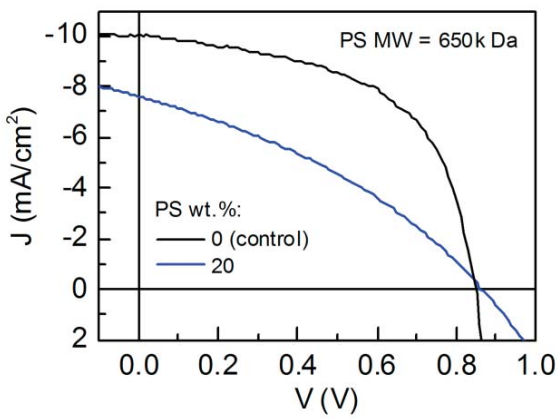

Figure S1. Representative J-V characteristics of PCDTBT:PCBM BHJ solar cells having either 0 wt.% (control) or 20 wt.% tertiary PS additives (MW = 650k Da), measured under 1 Sun AM1.5G illumination condition.

Table S1. Average device photovoltaic performance parameters of PCDTBT:PCBM BHJ solar cells either 0 wt.% (control) or 20 wt.% tertiary PS additives (MW = 650k Da))

PS wt.%	J_{sc} [mA/cm^2]	V_{oc} [V]	FF	PCE [%]
0 (control)	10.0 ± 0.3	0.84 ± 0.01	0.57 ± 0.02	4.8 ± 0.1
20	7.6 ± 0.4	0.85 ± 0.02	0.35 ± 0.03	2.3 ± 0.3

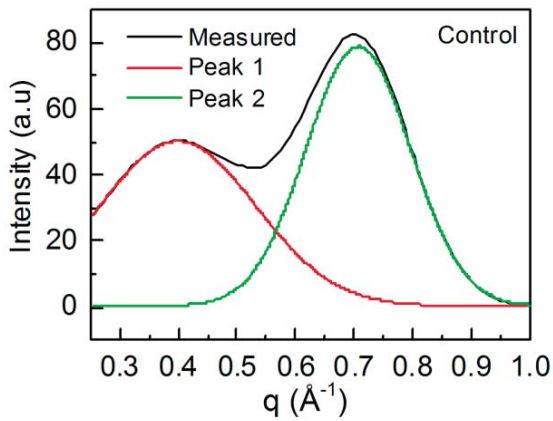

Figure S2. Representative peak deconvolution of the 1D GIWAXS intensity profile measured from a control PCDTBT:PCBM BHJ blend thin film by surface mode. Each deconvoluted peak follows a Gaussian function.

Table S2. Summary of deconvolution parameters for the 1D GIWAXS intensity profile at q ~ 0.4 Å^{-1} (corresponding to PCDTBT lamellar stacking), measured by either film or surface mode from PCDTBT:PCBM BHJ blend thin films having tertiary PS additives of various MWs

	Film mode				Surface mode			
PS MW [Da]	Peak center [Å^{-1}]	Peak area [a.u.]	FWHM [Å^{-1}]	Coherence length [2e]	Peak center [Å^{-1}]	Peak area [a.u.]	FWHM [Å^{-1}]	Coherence length [2e]
0[a)]	0.41	54.4	0.34	3.5	0.40	16.7	0.31	3.8
50k	0.41	61.9	0.36	3.3	0.41	27.4	0.37	3.2
1M	0.37	79.6	0.41	2.9	0.35	89.1	0.41	2.9
2M	0.36	84.9	0.42	2.8	0.38	112.4	0.40	3.0

[a)]Control sample without PS

Table S3. Summary of peak fitting parameters (Gaussian function) for the GIWAXS intensity profile at q ~ 1.38 Å^{-1} (corresponding to PCBM crystalline domains), measured by either film or surface mode from PCDTBT:PCBM BHJ blend thin films having tertiary PS additives of various MWs

	Film mode				Surface mode			
PS MW [Da]	Peak center [Å^{-1}]	Peak area [a.u.]	FWHM [Å^{-1}]	Coherence length [2e]	Peak center [Å^{-1}]	Peak area [a.u.]	FWHM [Å^{-1}]	Coherence length [2e]
0[a)]	1.38	192.6	0.26	4.5	1.39	62.8	0.27	4.3
50k	1.38	212.4	0.26	4.5	1.39	90.5	0.27	4.4
1M	1.38	268.8	0.27	4.3	1.38	411.0	0.30	4.0
2M	1.39	352.7	0.30	4.0	1.37	413.2	0.28	4.3

[a)]Control sample without PS

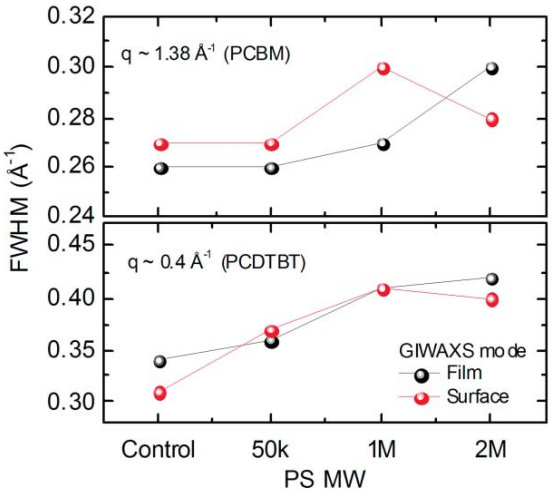

Figure S3. FWHM of GIWAXS peaks at q ~ 1.38 $Å^{-1}$ (corresponding to PCBM crystalline domains) and 0.4 $Å^{-1}$ (PCDTBT lamellar stacking) measured by either film or surface mode from PCDTBT:PCBM BHJ blend thin films having tertiary PS additives of various MWs. "Control" denotes the PCDTBT:PCBM blend without PS additive.

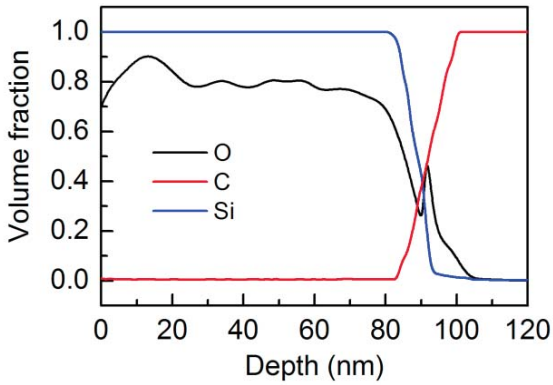

Figure S4. Typical composition depth-profile of a control PCDTBT:PCBM BHJ blend thin film spin-cast on a Si substrate, measured by TOF-SIMS.